

Luttinger liquids with boundaries: Power-laws and energy scales

V. Meden^{1,2}, W. Metzner¹, U. Schollwöck³, O. Schneider¹, T. Stauber², and K. Schönhammer²

¹ Institut für Theoretische Physik C, RWTH Aachen, D-52056 Aachen, Germany

² Institut für Theoretische Physik, Universität Göttingen, Bunsenstr. 9, D-37073 Göttingen, Germany

³ Sektion Physik, Universität München, Theresienstr. 37, D-80333 München, Germany

February 15, 2000

Abstract. We present a study of the one-particle spectral properties for a variety of models of Luttinger liquids with open boundaries. We first consider the Tomonaga-Luttinger model using bosonization. For weak interactions the boundary exponent of the power-law suppression of the spectral weight close to the chemical potential is dominated by a term linear in the interaction. This motivates us to study the spectral properties also within the Hartree-Fock approximation. It already gives power-law behavior and qualitative agreement with the exact spectral function. For the lattice model of spinless fermions and the Hubbard model we present numerically exact results obtained using the density-matrix renormalization-group algorithm. We show that many aspects of the behavior of the spectral function close to the boundary can again be understood within the Hartree-Fock approximation. For the repulsive Hubbard model with interaction U the spectral weight is enhanced in a large energy range around the chemical potential. At smaller energies a power-law suppression, as predicted by bosonization, sets in. We present an analytical discussion of the crossover and show that for small U it occurs at energies exponentially (in $-1/U$) close to the chemical potential, i.e. that bosonization only holds on exponentially small energy scales. We show that such a crossover can also be found in other models.

PACS. 71.10.-w Theories and models of many electron systems – 71.10.Pm Fermions in reduced dimensions

1 Introduction

Theoretically it is well established that interacting fermions in one spatial dimension do not obey Fermi liquid theory[1]. The generic low-energy physics of one-dimensional (1D) metallic fermions with repulsive interaction can be described by Luttinger liquid (LL) theory[1, 2, 3, 4, 5, 6]. For various correlation functions it predicts asymptotic power-law behavior with exponents which, for spin rotational invariant models, can be expressed in terms of a single parameter K_ρ . The Luttinger liquid parameter K_ρ depends on details of the model considered, e.g. the interaction, filling factor, and one-particle dispersion[6, 1]. It has been determined for many different models of 1D correlated electrons using either analytical or numerical techniques[7, 8, 1]. While the basic understanding of LL behavior emerged in the study of 1D systems with periodic boundary conditions (PBC), the theoretical expectation that LL's with PBC including impurities scale to chains with open ends[9, 10] led to several studies of models with hard walls, usually called “open” (or “fixed”) boundary conditions (OBC)[11, 12, 13, 14, 15]. One way to experimentally verify the predicted LL behavior is to probe the one-particle properties using high resolution photoemission spectroscopy. For the spectral function $\rho(\omega)$ entering the description of angular integrated photoemission and energies asymptotically close to the chemical potential μ , LL theory predicts

power-law suppression of the bulk spectral weight with an exponent

$$\alpha = (K_\rho + K_\rho^{-1} - 2)/(2z), \quad (1.1)$$

where $z = 1$ for spinless fermions and $z = 2$ for spin 1/2-fermions.

For the translational invariant system the scattering processes which dominate the low-energy physics can be classified as forward, backward, and umklapp scattering[5]. If the model parameters are such that backward or umklapp scattering become relevant in the renormalization-group (RG) sense both processes can drive the system into a gapped non-LL phase. In lattice models and for commensurate filling factors umklapp scattering becomes relevant at a critical value of K_ρ which depends on the filling. For the lattice models considered here we will always choose the interaction and filling such that umklapp scattering remains irrelevant. Standard RG arguments can be used[5] to show that for repulsive interactions the $2k_F$ -scattering part of the two-particle interaction (usually called “ g_1 -interaction”) scales to zero, where k_F denotes the Fermi wave vector. Then the Tomonaga-Luttinger (TL) model[2, 3] describes the generic low-energy LL physics. It only contains the scattering processes with small momentum transfer, which can be written as a quadratic form in bosonic density operators of left and right moving fermions.

This bosonization of the Hamiltonian is one of the ways to exactly solve the TL model with PBC[1,16]. For OBC we do not have momentum conservation and a general two-body interaction leads to a variety of different scattering vertices (see Sec. 2). They depend on different combinations (differences and sums) of the four external quantum numbers and cannot simply be parameterized by the “momentum transfer” as for PBC. Only a few of the vertices can be written as quadratic forms in boson operators similar to the case of PBC[2,5]. In some of the previous publications on the open boundary problem[11,12] it was tacitly assumed that RG arguments similar to the bulk case can be applied to show that the remaining vertices of the system without translational invariance scale to zero. Therefore a quadratic form in boson operators was used to describe the electron-electron interaction. Then it is straightforward to calculate correlation functions[11,12]. In Sec. 2 we present a detailed discussion of bosonization for the case of OBC taking all the scattering processes into account. We explicitly demonstrate that the above assumption is justified for an interaction which is long range in real space, considered by Tomonaga for PBC[2]. In Refs. [11] and [12] it was shown that the local spectral density $\rho(x,\omega)$ near the end points of a 1D chain is modified compared to the bulk density. The algebraic behavior of the spectral density with frequency ω close to the chemical potential was found to be governed by a *boundary exponent*

$$\alpha_B = (K_\rho^{-1} - 1)/z, \quad (1.2)$$

which, for repulsive interaction ($K_\rho < 1$), is larger than the bulk exponent α .

Systems of 1D correlated electrons can be viewed as being at a quantum critical point[1]. The occurrence of nonuniversal (critical) exponents can then be traced to the fact that the low-energy physics is governed by a line of fixed points. From the theory of critical phenomena it is known that critical exponents at a boundary usually differ from their bulk counterparts. Having this in mind the observed difference between α_B and α is not surprising[14].

To investigate whether Eq. (1.2) also characterizes the spectral function for models with OBC and a short range interaction we have calculated the spectral weight at the boundary site and the chemical potential using the density-matrix renormalization-group (DMRG) method[17] for the lattice model of spinless fermions with nearest neighbor interaction U and the 1D Hubbard model with onsite interaction U . In Secs. 5 and 6 we show that the numerically exact data are indeed consistent with Eq. (1.2), although for the Hubbard model only at energies extremely close to μ .

For small interactions and the models considered $K_\rho - 1$ can be expanded to give a leading behavior which is linear in the interaction[1,7,8]. For α this gives a leading term which is quadratic in the interaction. In second order perturbation theory for the self-energy the nonanalytic power-law behavior appears as a logarithmic divergence $\ln|\omega|$ with a prefactor which is of second order in the interaction[5]. In contrast α_B has a contribution *lin-*

ear in the interaction. Thus signs of the nonanalytic behavior of $\rho(x,\omega)$ can already be obtained using the (non-self-consistent) Hartree-Fock (HF) approximation for the self-energy. The least we can expect to find within the HF approximation is a logarithmic divergence of the above form with a prefactor linear in the interaction. In Secs. 4, 5, and 6 we study the spectral function for the three models (TL model, spinless fermions, Hubbard model) considered within the HF approximation. By comparison with the exact results (bosonization and DMRG) we show that many aspects of the low-energy behavior of $\rho(x,\omega)$ can be understood within the HF approximation. Surprisingly $\rho^{\text{HF}}(x,\omega)$ already gives power-law behavior. This is a very interesting observation as the HF approximation for the case of PBC does not capture any of the LL features.

Neither from general LL theory nor from the theoretical and numerical analysis of microscopic models, e.g. the 1D Hubbard model, much is known about the energy range Δ over which the power-law behavior in the spectral function can be observed. Obviously a knowledge of Δ is essential for a meaningful comparison of theoretical and experimental spectra. The analytical techniques used, e.g. bosonization and the Bethe Ansatz in combination with boundary conformal field theory[1], only provide the exponent which characterizes the spectral weight at energies *asymptotically* close to the chemical potential. This holds for both PBC and OBC. Quantum Monte-Carlo calculations of the spectral weight for the 1D Hubbard model with PBC indicate that Δ is small[18], which implies that chains of many lattice sites are required to observe the suppression in numerical calculations. In Sec. 6 we show that for the repulsive Hubbard model with OBC the spectral weight close to the boundary is *enhanced* in a large energy range around the chemical potential. The power-law suppression, predicted by bosonization, only occurs after a *crossover* at energies Δ which for small U are *exponentially* (in $-1/U$) close to the chemical potential. For the particular case considered this demonstrates that the bosonization (and conformal field theory) result only holds on a very small energy scale. We present an analytical discussion of the crossover behavior within an effective model. From perturbation theory we expect that this kind of crossover occurs in all models with a bare total backward scattering amplitude, i.e. z times the $2k_F$ component of the interaction, which is larger than the forward scattering.

Several attempts have been made to experimentally demonstrate LL behavior in a variety of systems which behave as quasi one-dimensional conductors using angular integrated and angular resolved photoemission spectroscopy[19,20,21,22,23]. Unfortunately all the measurements are plagued by various subtle problems[19] and their interpretation has been questioned[19,22]. Until three years ago the experimental spectra were compared to the predictions of bulk LL theory. Using the results obtained from bosonization and conformal field theory very recently many authors argued that the theoretical picture of a chain which, by impurities, is cut into several disconnected pieces gives a better agreement between the spectra ob-

served in photoemission experiments and theoretical spectra[12, 14, 19, 20, 23]. In Sec. 7 we will discuss this issue based on our results for the spectral function of the Hubbard model and the expectation that a crossover behavior similar to the one observed for the Hubbard model occurs also in other microscopic lattice models. Our results demonstrate that features which occur at energies not captured by bosonization and conformal field theory might dominate spectra broadened by finite temperatures and experimental resolution. Thus a reliable interpretation of photoemission data requires further theoretical investigations.

2 Open boundaries and bosonization

In this section we present a detailed discussion of bosonization for a continuum model of length L with OBC and a two-body interaction with a spatial range $R = 1/q_c$. We discuss the subtleties which in previous approaches have only partly been considered[11, 12].

The one-particle eigenstates of the noninteracting system are given by

$$\varphi_n(x) = \sqrt{2/L} \sin(k_n x), \quad (2.1)$$

with $k_n = n\pi/L$, $n \in \mathbf{N}$. Note that in contrast to the translational invariant case the k_n do not have the meaning of momenta. A 1D system with PBC has two Fermi points $\pm k_F$. In contrast here we only have one Fermi point given by $k_F = n_F \pi/L$, where zn_F [24] denotes the number of electrons in the system ($z = 1$ for spinless fermions and $z = 2$ for spin 1/2-fermions). The interaction between two particles of spin species s and s' is characterized by a two-body potential $V_{s,s'}(x-x')$ which leads to a contribution to the Hamiltonian given by

$$\begin{aligned} \hat{V} &= \frac{1}{2} \sum_{s,s'} \int_0^L dx \int_0^L dx' \psi_s^\dagger(x) \psi_{s'}^\dagger(x') \\ &\quad \times V_{s,s'}(x-x') \psi_{s'}(x') \psi_s(x) \\ &= \frac{1}{2} \sum_{s,s'} \int_0^L dx \int_0^L dx' \hat{\rho}_s(x) V_{s,s'}(x-x') \hat{\rho}_{s'}(x') \\ &\quad - \frac{1}{2} \sum_s V_{s,s}(0) \hat{N}_s, \end{aligned} \quad (2.2)$$

with the field operators $\psi_s^{(\dagger)}(x) = \sum_{n=1}^{\infty} \varphi_n(x) a_{n,s}^{(\dagger)}$, the density operators $\hat{\rho}_s(x) = \psi_s^\dagger(x) \psi_s(x)$, and the particle number operators $\hat{N}_s = \int_0^L dx \hat{\rho}_s(x)$. We express the interaction in terms of the creation and annihilation operators $a_{n,s}^{(\dagger)}$ of the eigenstates φ_n with spin s . After rearranging the terms in a way which simplifies the bosonization discussed later it reads

$$\begin{aligned} \hat{V} &= \frac{1}{2} \sum_{s,s'} \left[\sum_{n \neq n'} \sum_{m \neq m'} v_{nmm'n'}^{s,s'} a_{n,s}^\dagger a_{n',s}^\dagger a_{m,s'} a_{m',s'} \right. \\ &\quad \left. + \sum_{n \neq n'} \sum_m v_{nmm'n}^{s,s'} (a_{n,s}^\dagger a_{n',s} n_{m,s'} + \text{h.c.}) \right] \end{aligned}$$

$$+ \sum_{n,m} v_{nmm'n}^{s,s'} n_{n,s} n_{m,s'} - \delta_{s,s'} V_{s,s}(0) \hat{N}_s \Big], \quad (2.3)$$

with the matrix elements

$$\begin{aligned} v_{nmm'n'}^{s,s'} &= \int_0^L dx \int_0^L dx' \varphi_n^*(x) \varphi_{n'}(x) \\ &\quad \times V_{s,s'}(x-x') \varphi_m^*(x') \varphi_{m'}(x') \end{aligned} \quad (2.4)$$

and the occupation number operators $n_{n,s} = a_{n,s}^\dagger a_{n,s}$. If we express products of the sine functions φ_n in terms of cosine functions they read

$$\begin{aligned} v_{nmm'n'}^{s,s'} &= [F_{s,s'}(k_n - k_{n'}, k_m - k_{m'}) \\ &\quad - F_{s,s'}(k_n - k_{n'}, k_m + k_{m'}) - F_{s,s'}(k_n + k_{n'}, k_m - k_{m'}) \\ &\quad + F_{s,s'}(k_n + k_{n'}, k_m + k_{m'})] / L, \end{aligned} \quad (2.5)$$

with

$$\begin{aligned} F_{s,s'}(q, q') &= \frac{1}{L} \int_0^L dx \int_0^L dx' \cos(qx) V_{s,s'}(x-x') \\ &\quad \times \cos(q'x') \\ &= \frac{1}{4L} \iint_D dx dx' \left\{ e^{i(qx - q'x')} + e^{i(qx + q'x')} \right\} \\ &\quad \times V_{s,s'}(x-x'). \end{aligned} \quad (2.6)$$

The area D over which we have to integrate in Eq. (2.6) is given by the two hatched squares shown in Fig. 2.1 each of size L^2 . Using the fact that $V_{s,s'}(x)$ was assumed to have a range R , $F_{s,s'}(q, q')$ can partly be expressed in terms of the Fourier transform $\tilde{V}_{s,s'}(q) = \int_{-L}^L dx V_{s,s'}(x) \exp(-iqx)$ if we instead integrate over the rectangle of width $2R$ indicated in Fig. 2.1. This can be achieved by adding and subsequently subtracting the integral over the six black triangles. If we denote their contribution by $-g_{s,s'}(q, q')/L$, we obtain

$$F_{s,s'}(q, q') = \tilde{V}_{s,s'}(q)/2 (\delta_{q,q'} + \delta_{q,-q'}) + g_{s,s'}(q, q')/L. \quad (2.7)$$

In the case of a spin independent exponential interaction $V(x) = V_0/(2R) \exp(-|x|/R)$, $g(q, q')$ is proportional to $\tilde{V}(q)\tilde{V}(q')/V_0$.

For comparison we give a brief discussion of the interaction part of the Hamiltonian for the 1D electron gas with PBC. The noninteracting eigenstates are plane waves $\phi_n(x) = \exp(i\tilde{k}_n x)/\sqrt{L}$ with $\tilde{k}_n = 2\pi n/L$ and $n \in \mathbf{Z}$. In terms of the creation and annihilation operators $\tilde{a}_{n,s}^{(\dagger)}$ of these states a two-particle interaction gives a term similar to Eq. (2.3) with the matrix elements

$$\tilde{v}_{nmm'n'}^{s,s'} = \tilde{F}_{s,s'}(\tilde{k}_n - \tilde{k}_{n'}, \tilde{k}_m - \tilde{k}_{m'}) \quad (2.8)$$

and

$$\tilde{F}_{s,s'}(q, q') = \tilde{V}_{s,s'}(q) \delta_{q,-q'}/2. \quad (2.9)$$

For PBC the matrix elements thus only depend on the momentum transfer $\tilde{k}_n - \tilde{k}_{n'} = \tilde{k}_{m'} - \tilde{k}_m$ between the

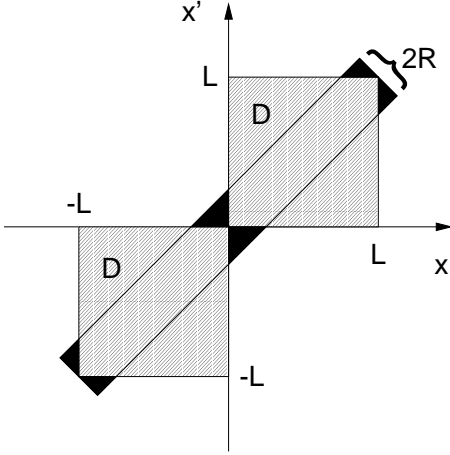


Fig. 2.1. Area of integration for the integral in Eq. (2.6). For details see the text.

two scattering particles. The part of the interaction with small momentum transfer $q \ll k_F$ can be written as a bilinear form in the spin and charge density operators of left and right moving fermions[2, 3, 16]. There are two ways of treating the backscattering processes with momentum transfer $2k_F$. One can show that for repulsive interactions backscattering is irrelevant in the RG sense[5]. If one is only interested in the “critical” low-energy properties of the model one can thus neglect backscattering from the beginning. Then the physical two-body potential has to be replaced by effective coupling constants, as it is changed by the initial flow of the backscattering and one ends up with an effective low-energy model[5]. The other way to proceed is to assume that the interaction $\tilde{V}_{s,s'}(q)$ is cut off at a momentum $q_c = 1/R \ll k_F$, i.e. is long range in real space and only consider a subspace of the Fock space \mathcal{F}_T with no holes deep in the Fermi sea and no particles in one-particle states with energies much higher than the Fermi energy. This is the idea originally considered by Tomonaga[2]. On this subspace the properly normalized density operators of left and right moving fermions obey bosonic commutation relations[16]. For a one-particle dispersion which is linearized around the two Fermi points also the kinetic energy is quadratic in the densities[16] and the entire Hamiltonian can be written as a Hamiltonian of noninteracting bosons.

From Eqs. (2.5) and (2.7) it is obvious that the situation is more complex for the case of OBC. Expressed in the basis of the noninteracting eigenstates the interaction contains a variety of scattering processes. Only a few of them can be written bilinearly in the density operators ($m \in \mathbf{Z}$, $m \neq 0$)

$$\rho_{m,s} = \sum_{n=\max\{1,1-m\}}^{\infty} a_{n,s}^\dagger a_{n+m,s}, \quad (2.10)$$

which obey $\rho_{m,s}^\dagger = \rho_{-m,s}$. Alternatively charge and spin density operators

$$\rho_{m,\rho} = (\rho_{m,\uparrow} + \rho_{m,\downarrow})/\sqrt{2} \quad (2.11)$$

$$\rho_{m,\sigma} = (\rho_{m,\uparrow} - \rho_{m,\downarrow})/\sqrt{2} \quad (2.12)$$

can be used. These operators are defined in analogy to the case of PBC. A RG study which includes all the scattering vertices is still missing and we will thus follow the idea of Tomonaga to investigate whether this leads to a Hamiltonian bilinear in the densities similar to PBC. Thus we assume that the interaction $V_{s,s'}(x)$ is long range in real space and only consider the low-energy subspace \mathcal{F}_T . For simplicity we will furthermore focus on the case of a spin independent interaction $V_{s,s'}(x) = V(x)$. Acting on states $|\psi_T\rangle \in \mathcal{F}_T$ the interaction term \hat{V} simplifies because $a_{n,s}^\dagger a_{n',s} |\psi_T\rangle = 0$ for $0 < |n - n'| \leq n_c$, unless $k_{n'}$ is close to k_F . As, with our assumption about the range of the interaction, $F(q, q')$ is only nonzero if both arguments are smaller than q_c we can replace $v_{nmn'm'}$ in the first term on the right hand side of Eq. (2.3) by $F(k_n - k_{n'}, k_m - k_{m'})/L$. With similar arguments for the other contributions the interaction term on \mathcal{F}_T reads

$$\begin{aligned} \hat{V} = & \frac{1}{2L} \sum'_{n,n'} F_\rho(q_n, q_{n'}) \rho_{n,\rho} \rho_{n',\rho} \\ & + \frac{1}{L} \sum_{n>0} F_\rho(q_n, 0) \hat{N}_\rho (\rho_{n,\rho} + \rho_{-n,\rho}) \\ & - \frac{\sqrt{z}}{L} \sum_{n>0} \sum_{m>0} F_\rho(q_n, 2k_m) (\rho_{n,\rho} + \rho_{-n,\rho}) \\ & + \frac{1}{2L} F_\rho(0, 0) \hat{N}_\rho^2 - \frac{\sqrt{z}}{L} \sum_{m>0} F_\rho(0, 2k_m) \hat{N}_\rho \\ & - \frac{\sqrt{z}}{2} V_\rho(0) \hat{N}_\rho + \frac{1}{L} \sum_{m,m'>0} F_\rho(2k_m, 2k_{m'}), \end{aligned} \quad (2.13)$$

with

$$\hat{N}_\rho = (\hat{N}_\uparrow + \hat{N}_\downarrow)/\sqrt{2}, \quad (2.14)$$

$$F_\rho(q, q') = z F_{s,s'}(q, q'), \quad (2.15)$$

$$V_\rho(0) = z V_{s,s'}(0). \quad (2.16)$$

The prime at the sum in Eq. (2.13) indicates that the terms with $n = 0$ or $n' = 0$ are excluded. For $z = 1$ the above formulas give the corresponding expressions for the case of spinless fermions, if one puts $\rho_{n,\rho} \rightarrow \rho_n$ and $\hat{N}_\rho \rightarrow \hat{N}$. Compared to the analogous expression for PBC[16] Eq. (2.13) contains three modifications: Generically $F_\rho(q_n, q_{n'})$ is nonvanishing for all q_n and $q_{n'}$ smaller than q_c which leads to a coupling between all the $\rho_{n,\rho}$ in the first line of Eq. (2.13)[11]. For PBC only $\rho_{n,\rho}$ with $n = -n'$ are coupled. OBC furthermore lead to a term which couples the particle number and the density operators and a term linear in the $\rho_{n,\rho}$ [25]. As we will discuss in Sec. 3 the latter leads to a nontrivial contribution to the Hartree term in the self-energy. For the discussion of the one-particle properties the constant as well as terms linear in \hat{N}_ρ can be neglected as the latter only lead to a renormalization of the chemical potential[16]. If we linearize the dispersion around k_F and for $n > 0$ define $b_{n,\nu} = \rho_{n,\nu}/\sqrt{n}$ for

$\nu = \rho, \sigma$ the kinetic energy on \mathcal{F}_T can, up to particle number contributions, be replaced by

$$\hat{H}_0 = v_F \frac{\pi}{L} \sum_{n>0} n (b_{n,\rho}^\dagger b_{n,\rho} + b_{n,\sigma}^\dagger b_{n,\sigma}) \quad (2.17)$$

with the Fermi velocity v_F . On \mathcal{F}_T the $b_{n,\rho/\sigma}$ obey bosonic commutation relations and charge and spin degrees of freedom do commute. Note that in $\hat{H} = \hat{H}_0 + \tilde{V}$ similar to PBC spin and charge degrees of freedom are decoupled. Formally a Hamiltonian \hat{H} of coupled and shifted harmonic oscillators can be diagonalized using a Bogoljubov transformation. For a general interaction the transformation cannot be given analytically, but e.g. for the above mentioned interaction $V(x) = V_0/(2R) \exp(-|x|/R)$, exploiting the fact that the corresponding $g(q, q')$ is separable, it can analytically be shown that neither the coupling of bosons with $|q_n| \neq |q_{n'}$ given by $g(q_n, q_{n'})$ nor the terms linear in the bosons do change the ‘‘critical’’ one-particle properties of the model, i.e. the exponents of the asymptotic decay of correlation functions[25]. As long as we are only interested in the ‘‘critical’’ behavior we can thus work with the simplified Hamiltonian

$$\begin{aligned} \hat{H} = & \sum_{n>0} n \left[v_F \frac{\pi}{L} b_{n,\rho}^\dagger b_{n,\rho} + \frac{z}{4L} \tilde{V}(q_n) (b_{n,\rho}^\dagger + b_{n,\rho})^2 \right] \\ & + v_F \frac{\pi}{L} \sum_{n>0} n b_{n,\sigma}^\dagger b_{n,\sigma}. \end{aligned} \quad (2.18)$$

In the following we will denote the model related to this Hamiltonian the TL model, even though we have dropped terms compared to Eq. (2.13) as described above. To obtain the spinless model from Eq. (2.18) one has to drop the second line and set $z = 1$. The TL model with OBC consists of an independent system of selfcoupled oscillators. This is in contrast to the PBC case, where the modes n and $-n$ are coupled by the interaction term. Apart from a constant Eq. (2.18) can be brought into the form[11, 16]

$$\hat{H} = \sum_{n>0} \left[\omega_n \alpha_{n,\rho}^\dagger \alpha_{n,\rho} + v_F \frac{\pi}{L} n b_{n,\sigma}^\dagger b_{n,\sigma} \right], \quad (2.19)$$

with $\omega_n = k_n \sqrt{1 + z\tilde{V}(k_n)/(\pi v_F)}$ and bosonic operators $\alpha_{n,\rho}$ given by a linear combination of $b_{n,\rho}^\dagger$ and $b_{n,\rho}$.

The one-particle spectral function $\rho^<(x, \omega)$ relevant for photoemission can be determined from the Green’s function $G^<(x, x, t) = -i \langle \psi_s^\dagger(x, 0) \psi_s(x, t) \rangle$ using[26]

$$\rho^<(x, \omega) = \int_{-\infty}^{\infty} \frac{dt}{2\pi} e^{i\omega t} iG^<(x, x, t). \quad (2.20)$$

Here $\langle \dots \rangle$ denotes the ground state expectation value. For the TL model with OBC $G^<(x, x, t)$ can be calculated using the bosonization of the fermionic field operator

$$\begin{aligned} \psi_s(x) &= \sqrt{\frac{2}{L}} \sum_{n=1}^{\infty} \sin(k_n x) a_{n,s} \\ &= \frac{-i}{\sqrt{2L}} \sum_{n=1}^{\infty} [e^{ik_n x} - e^{-ik_n x}] a_{n,s}. \end{aligned} \quad (2.21)$$

Eq. (2.21) cannot directly be expressed in the bosons $b_{n,\rho}^{(\dagger)}$ and $b_{n,\sigma}^{(\dagger)}$. To achieve this we have to add one-particle states with quantum numbers k_n , $n < 1$ to the Hilbert space. They are assumed to be filled in the ground state and do not modify the low-energy physics of the model. The auxiliary field operator

$$\tilde{\psi}_s(x) = \frac{1}{\sqrt{L}} \sum_{n=-\infty}^{\infty} e^{ik_n x} a_{n,s} \quad (2.22)$$

can then be written in the boson operators similar to PBC[16] and $G^<(x, x, t)$ is given by

$$\begin{aligned} G^<(x, x, t) = & \left[\langle \tilde{\psi}_s^\dagger(x, 0) \tilde{\psi}_s(x, t) \rangle + \langle \tilde{\psi}_s^\dagger(-x, 0) \tilde{\psi}_s(-x, t) \rangle \right. \\ & \left. - \langle \tilde{\psi}_s^\dagger(x, 0) \tilde{\psi}_s(-x, t) \rangle - \langle \tilde{\psi}_s^\dagger(-x, 0) \tilde{\psi}_s(x, t) \rangle \right] / 2. \end{aligned} \quad (2.23)$$

The expectation values in Eq. (2.23) can be calculated using bosonization of the auxiliary field operator[16]. For a fixed position x the leading behavior of $G^<(x, x, t)$ at large times is[11]

$$G^<(x, x, t) \sim t^{-(1+\alpha_B)} \quad (2.24)$$

with

$$\alpha_B = (K_\rho^{-1} - 1)/z \quad (2.25)$$

and the LL parameter

$$K_\rho = \left[1 + \frac{z\tilde{V}(0)}{\pi v_F} \right]^{-1/2} \quad (2.26)$$

of the TL model. The nonanalytic behavior of the spectral function close to the chemical potential is thus given by

$$\rho^<(x, \omega) \sim |\omega|^{\alpha_B} \Theta(-\omega). \quad (2.27)$$

Without explicitly demonstrating that the TL model is the effective low-energy model (fixed point model) for all models of LL’s with OBC the results of Eqs. (2.25) and (2.27) have been assumed to hold for all LL’s[11, 12]. This implies that the boundary exponent α_B can be expressed in terms of the bulk LL parameter K_ρ . The generalization found some confirmation in Ref. [13] where methods of boundary conformal field theory were used to calculate α_B for Bethe ansatz solvable models. In Sec. 5 we will present numerically exact results for the spectral weight of the lattice model of spinless fermions with nearest neighbor interaction, which are consistent with Eq. (2.27) over a fairly large energy range. Our results for the Hubbard model presented in Sec. 6 demonstrate that in this model the spectral function displays a richer structure. Only for energies Δ exponentially (in $-1/U$) close to μ , i.e. exponentially large system sizes, the small U data are consistent with Eq. (2.27).

Within the TL model and for fixed interaction strength the x dependence of the energy range Δ over which the asymptotic power-law suppression with the boundary exponent α_B can be observed is given by

$\Delta \approx v_F \min\{1/x, 1/R\}$. For $x > R$ and $v_F/x < \omega < v_F/R$ the bulk ‘‘critical’’ behavior with a power-law suppression given by α defined in Eq. (1.1) is recovered. For $\omega > v_F/R$ ‘‘nonuniversal’’ features dominate the spectrum. Unfortunately the energy scales obtained from the TL model cannot be trusted if one is interested in more realistic continuum or lattice models with a nonlinear one-particle dispersion and scattering processes given by a general interaction (not necessarily long range in real space). The best bosonization can provide for such models is the exponent of the nonanalytic behavior at energies asymptotically close to μ .

For small $\tilde{V}(0)$ it follows from Eq. (2.26) that

$$K_\rho = 1 - \frac{z\tilde{V}(0)}{2\pi v_F} + \mathcal{O}\left(\left[\frac{\tilde{V}(0)}{\pi v_F}\right]^2\right) \quad (2.28)$$

and thus from Eq. (2.25) that

$$\alpha_B = \frac{\tilde{V}(0)}{2\pi v_F} + \mathcal{O}\left(\left[\frac{\tilde{V}(0)}{\pi v_F}\right]^2\right) \quad (2.29)$$

This has to be contrasted to the small $\tilde{V}(0)$ behavior of the bulk exponent α Eq. (1.1) which is quadratic in the interaction. Thus signs of the nonanalytic behavior of $\rho(x, \omega)$ can already be obtained using the HF self-energy, which will be analysed in detail in the next section.

3 Hartree-Fock self-energy

In this section we discuss the non-self-consistent HF approximation for the self-energy $(\Sigma_s^{\text{HF}})_{n,n'}$, for the continuum model defined by Eq. (2.2) and a one-particle dispersion $\varepsilon(k)$. In contrast to the end of the last section we do not restrict our discussion to the subspace \mathcal{F}_T and thus consider all the scattering processes given by the Eqs. (2.3) to (2.7). We assume that the interaction is spin independent. For PBC $(\Sigma_s^{\text{HF}})_{n,n'} \propto \delta_{n,n'}$ because of momentum conservation and the HF approximation only leads to finite shifts in μ and v_F . It does not capture any of the peculiar properties of LL's. As already mentioned following Eq. (2.17) $g_{s,s'}(q, q')/L$ in Eq. (2.7) does not contribute to the ‘‘critical’’ LL properties of the continuum model with OBC. Later we will confirm this using perturbation theory. We will thus neglect this term and only consider the δ terms in Eq. (2.7). With the matrix elements given by Eq. (2.5) this leads to

$$\begin{aligned} [\Sigma_s^{\text{HF}}]_{n,n'} &= \sum_{n''=1}^{n_F} \sum_{s'} \left(v_{nn''n'n''}^{s,s'} - v_{nn''n'n''}^{s,s'} \delta_{s,s'} \right) \quad (3.1) \\ &= \delta_{n,n'} \left\{ \delta\mu - \frac{1}{2L} \sum_{n_1=1}^{n_F} \left[\tilde{V}(k_n - k_{n_1}) + \tilde{V}(k_n + k_{n_1}) \right] \right\} \\ &+ \frac{1}{2L} \left\{ z\tilde{V}(k_n + k_{n'}) - \tilde{V}\left(\frac{k_n - k_{n'}}{2}\right) \right\} f\left(\frac{n+n'}{2}\right) \\ &- \frac{1}{2L} \left\{ z\tilde{V}(k_n - k_{n'}) - \tilde{V}\left(\frac{k_n + k_{n'}}{2}\right) \right\} f\left(\frac{|n-n'|}{2}\right), \end{aligned}$$

with

$$f(m) = \begin{cases} 1 & \text{for } m \in \{1, 2, \dots, n_F\} \\ 0 & \text{otherwise} \end{cases} \quad (3.2)$$

and $\delta\mu = z\tilde{V}(0)n_F/L$. Due to the parity symmetry with respect to the middle of the box only matrix elements with even $n \pm n'$ are nonvanishing. Note that the self-energy is ω independent and real but has a nontrivial matrix structure in the quantum numbers n and n' due to the broken translational invariance. From the self-energy the retarded Green's function follows by a matrix inversion[26]

$$[G(\omega)]_{n,n'} = [\{\omega - \xi(k_n) + i0\} \mathbf{1} - \Sigma]_{n,n'}^{-1}, \quad (3.3)$$

with the unity matrix $\mathbf{1}$ and $\xi(k) = \varepsilon(k) - \mu$. The local spectral function is then given by

$$\rho(x, \omega) = -\frac{1}{\pi} \text{Im} \sum_{n,n'=1}^{\infty} \varphi_n^*(x) \varphi_{n'}(x) [G(\omega)]_{n,n'}. \quad (3.4)$$

$\rho^<(x, \omega)$ defined in Eq. (2.20) is related to the total spectral function of Eq. (3.4) by $\rho^<(x, \omega) = \rho(x, \omega)\Theta(\omega)$. To specify the model we have to choose a dispersion $\varepsilon(k)$ which is assumed to be sufficiently smooth. In the thermodynamic limit the noninteracting spectral weight is given by[27]

$$\rho^0(x, \omega) = \frac{1}{\pi} \left| \frac{d\varepsilon(k)}{dk} \right|^{-1} \left[1 - \cos(2kx) \right]_{k=\xi^{-1}(\omega)}, \quad (3.5)$$

where $\xi^{-1}(\omega)$ denotes the function inverting $\xi(k)$. We did not succeed in analytically inverting the matrix $[G^{\text{HF}}(\omega)]^{-1}$ in Eq. (3.3) which, for a general interaction, has a nontrivial structure. To gain a first insight in the behavior of the spectral weight close to μ the matrix can be inverted perturbatively to lowest order in \tilde{V}

$$\begin{aligned} \rho^{\text{HF}}(x, \omega) &= \rho^0(x, \omega) \left\{ 1 + \left[\frac{\tilde{V}(0)}{2\pi v_F} - z \frac{\tilde{V}(2k_F)}{2\pi v_F} \right] \right. \\ &\quad \left. \times \ln \left| \frac{\omega}{v_F k_F} \right| + \mathcal{O}(\tilde{V}^2) \right\}. \quad (3.6) \end{aligned}$$

Note that the logarithmic divergence in $\rho^{\text{HF}}(x, \omega)$ is not due to a singular frequency behavior of Σ^{HF} , but emerges in the perturbative approach to the matrix inversion. This has to be contrasted to PBC where the first indication of a break down of perturbation theory can be found in second order. The second order self-energy $\Sigma^{(2)}$ displays a logarithmic divergence $\tilde{V}^2 \ln |\omega|$ leading to the same kind of divergence in the spectral function[5, 16]. The diagram responsible for the second order divergence for PBC does also lead to a logarithmic divergence

$$[\Sigma_s^{(2)}(\omega)]_{n,n'} \sim \delta_{n,n'} \tilde{V}^2 \ln |\omega| \quad (3.7)$$

for OBC. Thus *logarithmic* terms found in perturbation theory for $\rho(x, \omega)$ in the case of OBC can have *two different origins*.

The leading logarithmic behavior in $\rho^{\text{HF}}(x, \omega)$ Eq. (3.6) comes from the term in Σ^{HF} which is proportional to $f(|n + n'|/2)$. It gives a sharp step in the self-energy matrix [see Eq. (3.2)] which crosses the diagonal at (n_F, n_F) . The height of the step determines the prefactor of the logarithmic divergence. Contributions of $g(q, q')$ neglected in Eq. (3.1) are continuous and thus do not modify the non-analytic behavior, consistent with the observation made in the last section. In Sec. 6 we will calculate the HF self-energy for the Hubbard model with OBC and present an analytical discussion of the resulting spectral weight in an effective model. Sharp steps in the HF self-energy matrix will also play a prominent role in this discussion.

To investigate how the leading logarithmic divergence of $\rho^{\text{HF}}(x, \omega)$ Eq. (3.6) is modified by higher orders in \tilde{V} , we numerically invert $[G^{\text{HF}}(\omega)]^{-1}$ for different models of finite size in Secs. 4, 5, and 6. It turns out that already the HF approximation leads to a power-law. We will furthermore compare the spectral weight in the HF approximation to exact results obtained from bosonization and DMRG.

4 Tomonaga-Luttinger model

The spectral function for the TL model of finite length L defined by Eq. (2.18) can be calculated exactly using bosonization and a recursive method introduced in Ref. [28] for the case of PBC. For the momentum integrated spectral function of the TL model the spin only leads to factors of two and we will thus consider the spinless TL model. The last two terms in Eq. (2.23) give contributions to $\rho(x, \omega)$ which for energies close to the chemical potential are proportional to $\cos(2k_F x)$. Such a term is already present in the noninteracting spectral function Eq. (3.5). It drops out if the spectral function is spatially averaged over a small length. If one is interested in the comparison to experimental spectra this assumption is justified as photoemission measurements will automatically average over some small spatial range. In Fig. 4.1 only the nonoscillatory part $\rho_{\text{no}}(x, \omega)$ of $\rho(x, \omega)$ is shown (solid line) as a function of ω . The low-energy behavior is independent of the shape of the interaction and we have chosen the simple form $\tilde{V}(q) = U\Theta(q_c - |q|)$. For a finite system $\rho(x, \omega)$ is given by a sum of δ peaks. In Fig. 4.1 the energies with nonvanishing weight are equidistant with a level spacing $\propto 1/L$ and we have connected them to a continuous line. A power-law behavior of the weight close to μ can only be found in the thermodynamic limit, but for large system sizes the weight of the δ peaks resembles the power-law obtained for $L \rightarrow \infty$. The data in Fig 4.1 display the suppression of spectral weight close to μ which is much stronger than the one observed for PBC. For comparison PBC data for the same parameters are shown in Fig. 4.1 as a dashed-dotted line.

The HF self-energy for the TL model differs for the two choices Eqs. (2.13) and (2.18) for the interaction. The term proportional to $\tilde{V}(k_n - k_{n'})f(|n - n'|/2)$ in Eq. (3.1) is due to the interaction term linear in the bosons neglected in

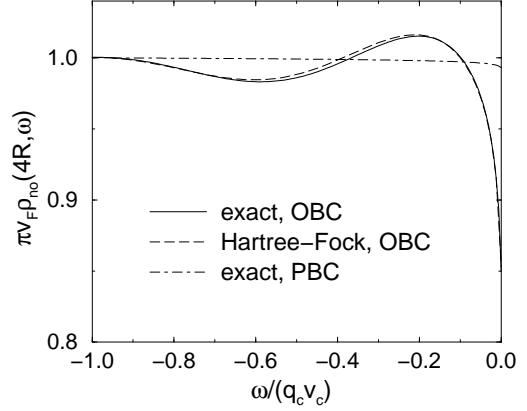


Fig. 4.1. Spectral weight near the boundary ($x = 4R$) for the spinless TL model with $U/(2\pi v_F) = 0.05263$, $n_c \equiv q_c L/\pi = 160$, and $n_F = 4n_c$.

Eq. (2.18). As it does not contribute to the singular part of the HF spectral function we treat the HF approximation to the TL model Eq. (2.18). This leads to

$$[\Sigma^{\text{HF}}]_{n, n'} = \delta_{n, n'} \left\{ z \frac{n_F}{L} \tilde{V}(0) - \frac{1}{2L} \sum_{n_1=1}^{n_F} \tilde{V}(k_n - k_{n_1}) \right\} - \frac{1}{2L} \tilde{V} \left(\frac{k_n - k_{n'}}{2} \right) f \left(\frac{n + n'}{2} \right). \quad (4.1)$$

The first term in Eq. (4.1) is the HF shift of the chemical potential and the second term leads to a renormalized Fermi velocity $v_{\text{HF}} = v_F + \tilde{V}(0)/(2\pi)$. The resulting matrix $[G^{\text{HF}}]^{-1}$ which has to be inverted is sketched in Fig. 4.2. If we consider the box shaped potential $\tilde{V}(q) = U\Theta(q_c - |q|)$ the last term in Eq. (4.1) does contribute as a constant in the hatched area. In Fig. 4.1 $\rho_{\text{no}}^{\text{HF}}(x, \omega)$ is shown as the dashed line. For the parameters chosen (weak interaction) the HF result agrees quantitatively with the exact solution. For the TL model $\tilde{V}(2k_F) = 0$, which leads to [see Eq. (3.6)]

$$\rho^{\text{HF}}(x, \omega) \sim 1 + \frac{\tilde{V}(0)}{2\pi v_F} \ln \left| \frac{\omega}{v_F k_F} \right| + \dots \quad (4.2)$$

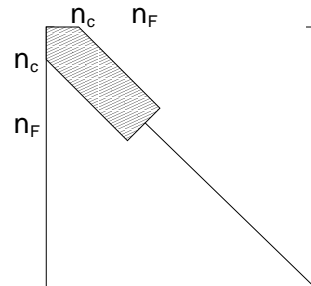


Fig. 4.2. $[G^{\text{HF}}]^{-1}$ for the TL model. For details see the text.

For repulsive interactions ($\tilde{V}(0) > 0$) the prefactor of the logarithm is positive and the perturbative expression indicates a suppression of the weight. To further investigate the behavior of $\rho(x, \omega)$ close to the chemical potential we have studied the spectral weight at the chemical potential and position x , denoted $w_0(x, n_F; \tilde{V})$, for a given k_F as a function of $1/n_F$ ($\propto 1/L$). The ratio $w_0(x, n_F; \tilde{V})/w_0(x, n_F; 0)$ displays the same kind of power-law behavior as does $\rho(x, \omega)$ as a function of ω . Smaller systems are sufficient to find power-law behavior in $w_0(x, n_F; \tilde{V})/w_0(x, n_F; 0)$ compared to $\rho(x, \omega)$. Fig. 4.3 shows a log-log plot of $w_0(x, n_F; \tilde{V})/w_0(x, n_F; 0)$ for the exact solution and the HF approximation. A power-law fit of the symbols gives the expected exponent Eqs. (2.25) and (2.26) with high accuracy. Surprisingly also the HF approximation displays power-law behavior, which shows that the leading logarithmic divergence of ρ^{HF} found in Eq. (4.2) can be resummed to give a power-law. A detailed study shows that $\alpha_B^{\text{HF}} = \tilde{V}(0)/(2\pi v_{\text{HF}})$ and thus α_B^{HF} and α_B do agree up to leading order in $\tilde{V}(0)/(2\pi v_F)$. Quantitative agreement between exact results and HF can be reached for $\tilde{V}(0)/(2\pi v_F) \ll 1$.

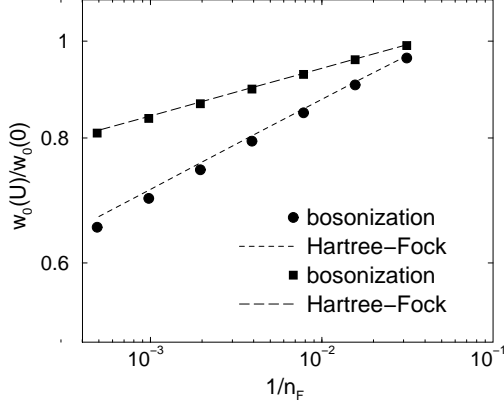


Fig. 4.3. Spectral weight at μ and close to the boundary. The circles show the exact results for the spinless TL model for $x = 3R$, $U/(2\pi v_F) = 0.1$ and $k_F = 4q_c$. The long dashed line presents the HF approximation. The squares show the exact results for $x = 3R$ and $U/(2\pi v_F) = 0.05$ and the dashed line the corresponding HF approximation.

5 Lattice model of spinless fermions

Next we consider the lattice model of spinless fermions with N lattice sites, lattice constant $a = 1$, hopping matrix element $t = 1$, nearest neighbor interaction U , and OBC

$$\hat{H} = - \sum_{j=1}^{N-1} \left(c_j^\dagger c_{j+1} + c_{j+1}^\dagger c_j \right) + U \sum_{j=1}^{N-1} n_j n_{j+1}. \quad (5.1)$$

$c_j^{(\dagger)}$ denotes the creation (annihilation) operator at site j and $n_j = c_j^\dagger c_j$. For $U = 0$ the eigenstates of \hat{H} are given

by Eq. (2.1) with $L \rightarrow N+1$, $x \rightarrow j$ and $k_n = n\pi/(N+1)$, $n \in \{1, 2, \dots, N\}$. Similar to PBC the one-particle dispersion is $\varepsilon(k) = -2 \cos(k)$. In contrast to the TL model the interaction is of short range (in real space) and it is not obvious whether the bosonization result Eq. (2.25) $\alpha_B = K_\rho^{-1} - 1$ holds. As for PBC the interacting model with OBC can be solved exactly by the Bethe ansatz, but similar to PBC not much about correlation functions can be learned directly from the solution. Information about boundary exponents can be obtained if conformal invariance is assumed[13, 15].

Here we discuss the local spectral function at site $j = 1$. We have performed a DMRG study[17] for chains of up to $N = 512$ sites calculating matrix elements $w_0(n_F; U) = |\langle E_0^{n_F-1} | c_1 | E_0^{n_F} \rangle|^2$, i. e. the spectral weight at the chemical potential and the boundary site (see Sec. 4). $|E_0^{n_F}\rangle$ denotes the exact n_F -particle ground state. Results for $w_0(n_F; U)/w_0(n_F; 0)$ as a function of $1/N$ (instead of $1/n_F$), two different filling factors $n_f = n_F/N$, and U are shown as the symbols in Fig. 5.1. $K_\rho(U, n_f)$ for these parameters can e.g. be found in Ref. [8]: $K_\rho(U = 0.1, n_f = 0.5) = 0.9691$ and $K_\rho(U = 1, n_f = 0.25) = 0.8447$. For large N the numerical data nicely follow the solid lines, which are proportional to power-laws with exponent $\alpha_B(U = 1, n_f = 0.25) = 0.1838$ respectively $\alpha_B(U = 0.1, n_f = 0.5) = 0.0319$. The numerical error of the DMRG data is smaller than the size of the symbols. We can thus conclude that the spectral weight close to the boundary and the chemical potential shows a suppression with a power-law and exponent α_B . This is consistent with the prediction of bosonization and results presented in Ref. [13] obtained from Bethe ansatz and boundary conformal field theory.

In contrast to the TL model the HF problem for spinless fermions is numerically best studied in the site representation. The HF or mean-field Hamiltonian is given by

$$\begin{aligned} \hat{H}^{\text{HF}} = & - \sum_{j=1}^{N-1} \left(t(j) c_j^\dagger c_{j+1} + t^*(j) c_{j+1}^\dagger c_j \right) \\ & + \sum_{j=1}^{N-1} [U + u(j)] n_j \end{aligned} \quad (5.2)$$

with a renormalized hopping

$$\begin{aligned} t(j) &= 1 + U \langle c_{j+1}^\dagger c_j \rangle_0 \\ &= 1 + \frac{2U}{N+1} \sum_{n=1}^{n_F} \sin(k_n j) \sin(k_n [j+1]), \end{aligned} \quad (5.3)$$

onsite energies

$$u(j) = U \begin{cases} \langle n_2 \rangle_0 & \text{for } j = 1 \\ \langle n_{j-1} \rangle_0 + \langle n_{j+1} \rangle_0 & \text{for } j \in \{2, 3, \dots, N-1\} \\ \langle n_{N-1} \rangle_0 & \text{for } j = N, \end{cases}$$

and

$$\langle n_j \rangle_0 = \frac{2}{N+1} \sum_{n=1}^{n_F} \sin^2(k_n j), \quad (5.4)$$

where $\langle \dots \rangle_0$ denotes the noninteracting ground state expectation value. Due to the OBC the site occupation $\langle n_j \rangle_0$ depends on j showing Friedel oscillations. The sums in Eqs. (5.3) and (5.4) can be performed analytically and in order to obtain the site diagonal Green's function $[G^{\text{HF}}(\omega)]_{j,j}$, and thus the spectral function $\rho_j^{\text{HF}}(\omega)$, one numerically has to determine the eigenvalues and eigenvectors of a tridiagonal matrix. This can easily be done for systems of up to $N = 10^6$ lattice sites. Fig. 5.1 shows HF data for $w_0(n_F; U)/w_0(n_F; 0)$ and the same parameters as above. Similar to the TL model already the HF approximation displays power-law behavior with exponent $\alpha_B^{\text{HF}} = \tilde{V}_{\text{eff}}/(2\pi v_{\text{HF}})$ which has the same form as for the TL model if one replaces $\tilde{V}(0)$ by the effective interaction $\tilde{V}_{\text{eff}} = \tilde{V}(0) - \tilde{V}(2k_F) = 2U[1 - \cos(2k_F)]$. This replacement is familiar from the mapping to the “ g -ology” model for PBC[5]: For spinless fermions forward g_2 and backward g_1 scattering are indistinguishable which leads to an effective coupling $g_2 - g_1$. Again α_B and α_B^{HF} agree up to order $\tilde{V}_{\text{eff}}/(2\pi v_F)$ and both curves show quantitative agreement for $\tilde{V}_{\text{eff}}/(2\pi v_F) \ll 1$.

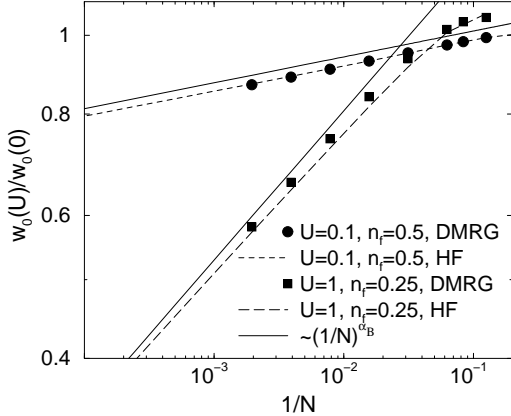


Fig. 5.1. Spectral weight at μ and lattice site 1 for the lattice model of spinless fermions. The symbols show the DMRG data and the dashed lines the corresponding HF results. For comparison the solid lines are power-laws with exponent $\alpha_B = K_\rho^{-1} - 1$. The parameters are given in the legend.

6 Hubbard model

The main part of our earlier publication[29] on LL's with boundaries is devoted to a numerical investigation of the spectral properties of the 1D repulsive Hubbard model

$$\hat{H} = - \sum_s \sum_{j=1}^{N-1} \left(c_{j,s}^\dagger c_{j+1,s} + c_{j+1,s}^\dagger c_{j,s} \right) + U \sum_{j=1}^{N-1} n_{j,\uparrow} n_{j,\downarrow}. \quad (6.1)$$

Similar to the lattice model of spinless fermions Eq. (5.1) we set the lattice constant a and the hopping matrix element t equal to unity. Here we will give a short summary of the numerical results obtained in Ref. [29], discuss new data sets, and then present an analytical investigation of the crossover behavior of the spectral weight within an effective low-energy model.

6.1 Numerical results: DMRG

As for the lattice model of spinless fermions we have calculated the spectral weight at the boundary site and the chemical potential as a function of the number of lattice sites N using the DMRG algorithm. We were able to obtain results for up to $N = 256$ sites. Figs. 6.1 and 6.2 show data for $w_0(n_F; U)/w_0(n_F; 0)$, quarter filling $n_f = 2n_F/N = 0.5$, and different U . The numerical error of the DMRG data is of the order of the symbol size. Instead of decreasing, as predicted by bosonization and in contrast to our findings for the other two models considered, $w_0(n_F; U)/w_0(n_F; 0)$ *increases* for small and moderate values of U (see Fig. 6.1). For moderate $U \approx 2$ a crossover to a suppression occurs at system sizes reachable within DMRG. For smaller U , e.g. $U = 0.5$, only the increase can be seen. We expect that the crossover sets in at much larger chain length. Only the large U data of Fig. 6.2 display a clear suppression of the spectral weight for all the system sizes available and thus only for these data a comparison to the power-law with exponent $\alpha_B = (K_\rho^{-1} - 1)/2$ predicted by bosonization seems meaningful. $K_\rho(U, n_f)$ for the Hubbard model has been calculated in Ref. [7]. For the parameters chosen we have $K_\rho(U = 8, n_f = 0.5) = 0.62$ and $K_\rho(U = 16, n_f = 0.5) = 0.56$. Power-laws with exponents $\alpha_B(U = 8, n_f = 0.5) = 0.31$ and $\alpha_B(U = 16, n_f = 0.5) = 0.39$ are shown as solid lines in Fig. 6.2. For large N the numerical data seem to approach these lines and we conclude that the DMRG results are consistent with a final power-law suppression of the spectral weight near the boundary which is given by the boundary exponent α_B . The asymptotic behavior is thus consistent with the prediction of bosonization[11, 12] and results obtained using Bethe ansatz and boundary conformal field theory[13].

The surprising new finding is the increase of weight for small and moderate U and the subsequent crossover. This could have been expected already from the lowest order result Eq. (3.6) for the spectral function. For a k -independent interaction U the leading logarithmic correction to ρ^H is given by[30]

$$\rho^H(x, \omega) \sim 1 + (1 - z) \frac{U}{2\pi v_F} \ln \left| \frac{\omega}{v_F k_F} \right| + \dots \quad (6.2)$$

The prefactor of the logarithmic correction in a model with spin ($z = 2$) has thus the opposite sign as in the case of a long range interaction Eq. (4.2). As long as $[U/(2\pi v_F)] \ln(N) \ll 1$ this indicates a logarithmic increase of the weight displayed in Fig. 6.1. The crossover scale can be estimated from this expression to be $1/N_c^A \sim$

$\exp[-2\pi v_F/U]$. From the data it is clear that also the exact crossover scale $1/N_c$ strongly depends on U . Going from $U = 2.5$ to $U = 2$ it roughly decreases by one order of magnitude. As a consequence of this and the fact that we are limited to $N = 256$ lattice sites the crossover can only be observed within a small window of interactions $2 \leq U \leq 3$. Below we will show that the crossover scale indeed decreases exponentially in $-1/U$ using our analytical Hartree result and scaling arguments. The $1/N$ dependence of $w_0(n_F; U)/w_0(n_F; 0)$ can be translated into the ω dependence of $\rho_1(\omega)$ by multiplying by the inverse of the noninteracting density of states πv_F . For the energy scale at which the decrease of the weight sets in we thus find $\Delta = v_F \pi / N_c$. For e.g. the $U = 2.5$ data at quarter filling this leads to $\Delta/B \approx 10^{-2}$, where B denotes the bandwidth $B = 4$. This implies that for the given parameters the prediction of bosonization only holds for energies much smaller than one hundredth of the bandwidth. In Sec. 7 we will further discuss this issue.

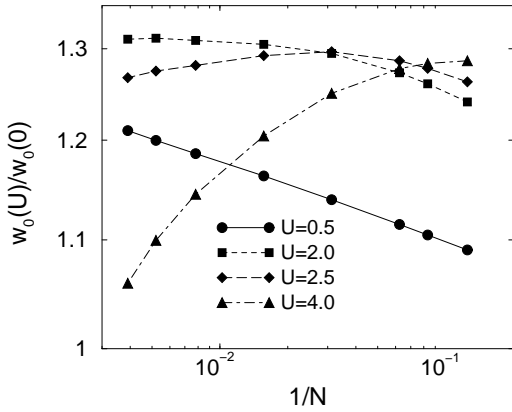


Fig. 6.1. DMRG results for the spectral weight at μ and lattice site 1 for the Hubbard model at quarter filling. The interaction U is given in the legend.

6.2 Numerical results: Hartree approximation

Numerically the Hartree approximation (the Fock term vanishes) for the Hubbard model is best studied in the site representation. It can be done in close analogy to the lattice model of spinless fermions discussed in Eqs. (5.2) to (5.4). For the Hubbard model the hopping is not modified by the interaction and the one-particle problem which remains to be solved for an electron of spin species s is the dynamics in an external Hartree potential generated by $\langle n_{j,-s} \rangle_0$. The Hartree potential shows Friedel oscillations, i.e. oscillates as $\cos(2k_F j)$ and slowly decays as $1/j$. In the continuum limit external potentials of this form are called Wigner-von Neumann type potentials[31]. From scattering theory it is known that the eigenvalues and eigenstates of Hamilton operators with oscillating and slowly decaying ($\sim 1/x$) external potentials have unusual properties[31].

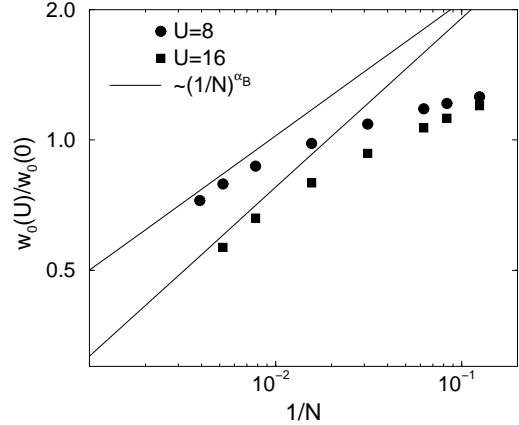


Fig. 6.2. The same as in Fig. 6.1, but for larger U . The solid lines are power-laws with exponent $\alpha_B = (K_\rho^{-1} - 1)/2$.

Numerically the spectral weight of the lattice model can be calculated along the lines discussed in the last section. In Figs. 2 and 3 of Ref. [29] we have presented numerical data for $\rho_1^H(\omega)$ as a function of ω , different U , and system sizes of up to $N = 10^6$ lattice sites. We have restricted ourselves to energies close to the chemical potential. For small and moderate U the spectra display qualitatively the same behavior as the DMRG data discussed above. For energies approaching the chemical potential from below the weight first increases following a power-law. From the numerical data the exponent can be determined with high accuracy to be $-U/(2\pi v_F)$. This shows that the logarithmic divergence Eq. (6.2) obtained in the leading order solution of the Hartree problem can be resummed to produce a power-law in an energy range close to the chemical potential. The numerical Hartree data then display a crossover on a scale which decreases exponentially in $-1/U$, and a subsequent power-law suppression. From the numerical data the exponent is found to be

$$\alpha_B^H = U/(2\pi v_F). \quad (6.3)$$

α_B^H has to be compared to the leading behavior of the exact boundary exponent $\alpha_B = (K_\rho^{-1} - 1)/2$. It is given by $\alpha_B = U/(4\pi v_F) + \mathcal{O}([U/2\pi v_F]^2)$ [32] which is one-half of α_B^H . This kind of discrepancy between exponents obtained in perturbation theory and the leading behavior of exact exponents is known from the Hubbard model with PBC[33]. It occurs because the scaling of coupling constants (of the backscattering contribution in case of PBC) is not taken into account in simple perturbation theory. Thus the coupling constant relevant for exponents is overestimated in a naive perturbative treatment. For the same reason DMRG and Hartree data only show qualitatively agreement even in the limit of small coupling (see Fig. 4 of Ref. [29]). This has to be contrasted to the above results for the TL model and the lattice model of spinless fermions. In analogy to PBC the couplings in these two models do not scale[5].

Fig. 6.3 shows $\rho_1^H(\omega)$ as a function of ω for all energies within the band, $N = 2000$, $U = 5$, and two fill-

ing factors n_f which are related by $n_f \rightarrow 2 - n_f$. The individual weights have been connected to a continuous line. Since the hopping amplitude is not renormalized by the interaction the total bandwidth is equal to the non-interacting one $B = 4$. Besides the crossover behavior for energies close to the chemical potential, i.e. $\omega = 0$, the solid line with $n_f = 0.8$ shows a symmetric suppression of weight around $\omega = -2\varepsilon(k_F) > 0$, i.e. at energies which are unoccupied in the ground state. On the Hartree level the spectral function shows two important symmetries. In the next subsection the reason for both, the suppression at $\omega = -2\varepsilon(k_F)$ and the symmetries will become clear. The spectral function for fixed filling and repulsive interaction $U > 0$ can be mapped onto the one for attractive interaction with the same absolute value $-|U|$ and the same filling by taking the mirror image at $\omega = -\varepsilon(k_F)$. In this way the weight for $U > 0$ around $\omega = -2\varepsilon(k_F)$ is mapped onto the one for $-|U|$ around $\omega = 0$, i.e. the chemical potential. Here we do not consider the spectral function for negative U any further since the Hubbard model with attractive interaction is not a LL[5,1]. The second symmetry is obvious from Fig. 6.3. The spectral function for fixed U and filling $n_f < 1$ can be mapped onto the one with filling $2 - n_f$ by taking the mirror image at $\omega = 0$. Note that the weight for $U > 0$ and energies around the chemical potential shows a strong asymmetry. It implies that for $n_f < 1$ the increase preceding the final suppression of the weight of energies which are occupied in the ground state is more pronounced compared to the analogous weight for fillings $n_f > 1$. This has to be contrasted to bosonization which always gives symmetric behavior around $\omega = 0$.

Next we will present an analytical discussion of the spectral weight within the Hartree approximation. We will be able to analytically determine the exponents of the power-law increase, the subsequent decrease and the crossover scale $\Delta(U, n_f)$ discussed above.

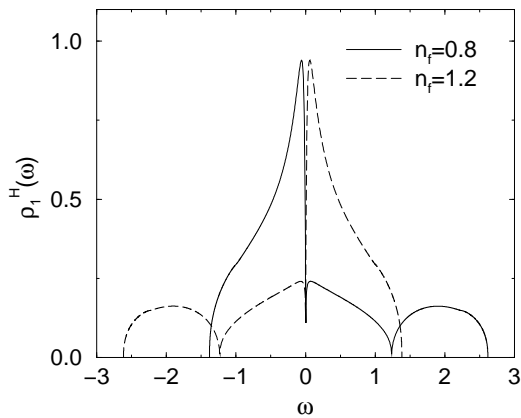


Fig. 6.3. Spectral function of the Hubbard model at site $j = 1$, for $N = 2000$, $U = 5$, and two different filling factors n_f in the Hartree approximation.

6.3 Analytical results

For an analytical discussion of the Hartree approximation it is preferable to work in k -space. Similar to the case of a general continuum model Eqs. (2.3) to (2.7) we thus first calculate the matrix elements of the local Hubbard interaction in the noninteracting eigenstates

$$\varphi_n(j) = \sqrt{\frac{2}{N+1}} \sin(k_n j), \quad (6.4)$$

with $k_n = n\pi/(N+1)$, $n \in \{1, 2, \dots, N\}$. They can be written similar to Eq. (2.5) with

$$\begin{aligned} F_{s,s'}(q_m, q_{m'}) &= \delta_{s,-s'} \frac{U}{N+1} \sum_{j=0}^N \cos(q_m j) \cos(q_{m'} j) \\ &= \delta_{s,-s'} \frac{U}{2} \left(\delta_{m,m'}^{(N+1)} + \delta_{m,-m'}^{(N+1)} \right), \end{aligned} \quad (6.5)$$

and the $(N+1)$ -periodic Kronecker δ , $\delta_{m,m'}^{(N+1)} = 1$ for $m = m' + l(N+1)$, $l \in \mathbf{Z}$ and zero otherwise. A comparison with Eq. (2.7) shows that the correction term $g(q, q')$ vanishes for a local interaction. From Eq. (6.5) the Hartree self-energy can be calculated. In Fig. 6.4 the self-energy matrix

$$\tilde{\Sigma}_s^H = \Sigma_s^H - \delta\mu \mathbf{1} \quad (6.6)$$

with $\delta\mu = U(n_f + 1/2)/(N+1)$, is sketched for a filling factor $n_f < 1$. Similar to the TL model the function $f([n+n']/2)$ Eq. (3.2) enters the expression for the self-energy and only matrix elements with even $n+n'$ do contribute. In the hatched area and for even $n+n'$ the matrix elements are given by $-U/[2(N+1)]$. They vanish outside this area. For half filling $n_f = 1$ all the off-diagonal elements of the self-energy matrix vanish and the spectral function is given by the noninteracting one. For fillings $n_f > 1$, $\tilde{\Sigma}_s^H$ is given as sketched in Fig. 6.4 but with $n_f \rightarrow N - n_f$ and $U \rightarrow -U$. This leads to the symmetries of the spectral weight discussed in the last subsection. From now on we will restrict ourselves to fillings $n_f < 1$. The weight for $n_f > 1$ can be constructed using the discussed symmetry. From the self-energy the Green's function $[G(\omega)]_{n,n'}$ can be calculated following Eq. (3.3).

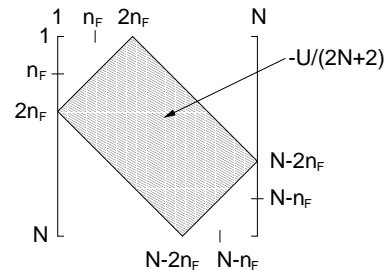


Fig. 6.4. The self-energy matrix $\tilde{\Sigma}_s^H$ for the Hubbard model with $n_f < 1$. For details see the text.

A lowest order inversion of $[G^H]^{-1}$ leads to Eq. (6.2). The calculation shows that the nonanalytic behavior of the

spectral function close to the chemical potential, i.e. close to $\omega = 0$, comes from the step through the point (n_F, n_F) in the upper left part of the self-energy matrix Fig. 6.4. It is given by the line $n' = 2n_F + 1 - n$. The sharp step in the lower right half, given by $n' = 2(N+1) - 2n_F - 1 - n$, comes from unklapp processes where $m = m' + N + 1$ in Eq. (6.5). In the spectral function it leads to the symmetric suppression of the weight close to the unoccupied energy $\omega = -2\varepsilon(k_F)$ already discussed in the last subsection (see the solid line in Fig. 6.3). Numerically it can be shown that the suppression is given by a power-law with exponent $U/(2\pi v_F)$.

6.3.1 Effective model

As we are only interested in the nonanalytic behavior of the spectral weight for energies close to the chemical potential the Hartree problem can be simplified. This leads to an effective low-energy model. Due to the structure of the self-energy matrix the Hartree problem separates into two equivalent problems. One for even n and n' and the other one for odd n and n' . In both problems the vanishing matrix elements in the hatched area of Fig. 6.4 are left out, but the level spacing is doubled. Equivalently one can work with a ‘‘coarse grained’’ version of $\tilde{\Sigma}_s^H$. It has nonvanishing matrix elements for all n and n' in the hatched area of Fig. 6.4, but they have only half the size of the original ones. As only the sharp step in the upper left part is important for the nonanalytic behavior close to μ the matrix $\tilde{\Sigma}_s^H$ can be replaced by a matrix \mathcal{V} with elements

$$\mathcal{V}_{n-n_F, n'-n_F} = -\frac{U}{4(N+1)} \Theta(n+n'-2n_F). \quad (6.7)$$

Next the space of one-particle states is changed. Without modifying the low-energy properties it can be reduced to $n \in \{1, 2, \dots, 2n_F\}$. Furthermore the one-particle dispersion $\xi(k)$ can be linearized around k_F

$$\xi(k - k_F) = v_F(k - k_F). \quad (6.8)$$

In a last step the quantum numbers n are shifted by n_F . We then have to determine the local spectral function for a scattering problem with the Hamiltonian

$$\hat{H}_{\text{eff}} = \sum_{n=-n_F+1}^{n_F} v_F k_n a_n^\dagger a_n + \sum_{n, n'=-n_F+1}^{n_F} \mathcal{V}_{n, n'} a_n^\dagger a_n \quad (6.9)$$

In order to obtain a continuous spectral function we take the thermodynamic limit. This is accomplished by switching to unperturbed one-particle states

$$\tilde{\varphi}_k(j) = \sqrt{\frac{2}{\pi}} \sin[(k_n + k_F)j]. \quad (6.10)$$

and using

$$\sum_n \longrightarrow \frac{N+1}{\pi} \int dk. \quad (6.11)$$

In these states the scattering potential is given by

$$\mathcal{V}_{k, k'} = -\frac{U}{4\pi} \Theta(k + k'). \quad (6.12)$$

6.3.2 Scattering theory

As usual in scattering theory[34] we define the off-shell T matrix $T(\omega)$ which obeys the Lippmann-Schwinger equation

$$T(\omega) = \mathcal{V} + \mathcal{V}G_0(\omega)T(\omega), \quad (6.13)$$

with the bare retarded Green's function

$$[G_0(\omega)]_{k, k'} = \frac{1}{\omega - v_F k + i0} \delta(k - k'). \quad (6.14)$$

The local spectral function can then be calculated from Eq. (3.4) and

$$G(\omega) = G_0(\omega) + G_0(\omega)T(\omega)G_0(\omega). \quad (6.15)$$

For the present problem it turns out to be advantageous to express the Green's function in terms of the so called K (or Heitler) matrix[34] which obeys the Lippmann-Schwinger equation

$$K(\omega) = \mathcal{V} + \mathcal{V}G_0^R(\omega)K(\omega), \quad (6.16)$$

with

$$[G_0^R(\omega)]_{k, k'} = \frac{\mathcal{P}}{\omega - v_F k} \delta(k - k'). \quad (6.17)$$

Here \mathcal{P} denotes the principal value. T and K are related by

$$[T(\omega)]_{k, k'} = [K(\omega)]_{k, k'} - i\pi \frac{[K(\omega)]_{k, \tilde{\omega}} [K(\omega)]_{\tilde{\omega}, k'}}{v_F + i\pi [K(\omega)]_{\tilde{\omega}, \tilde{\omega}}} \quad (6.18)$$

with $\tilde{\omega} = \omega/v_F$. Using Eqs. (6.15) and (3.4) this leads to

$$\rho_j^{\text{eff}}(\omega) = \rho_j^0(\omega) \frac{h_j(\omega)}{1 + \pi^2 g(\omega)}, \quad (6.19)$$

where the noninteracting spectral weight is given by Eq. (3.5)

$$\rho_j^0(\omega) = \frac{1 - \cos(2[k_F + \omega/v_F]j)}{\pi v_F}. \quad (6.20)$$

Close to the boundary and for $|\omega| \ll v_F k_F$, $\rho_j^0(\omega)$ can be replaced by its value at $\omega = 0$. The functions g and h_j are given by

$$g(\omega) = [K(\omega)]_{\tilde{\omega}, \tilde{\omega}}^2 / v_F^2 \quad (6.21)$$

and

$$h_j(\omega) = \left[1 + \mathcal{P} \int_{-k_F}^{k_F} dk \frac{\tilde{\varphi}_k(j)}{\tilde{\varphi}_{\tilde{\omega}}(j)} \frac{[K(\omega)]_{k, \tilde{\omega}}}{\omega - v_F k} \right]^2, \quad (6.22)$$

with $\tilde{\varphi}_k(j)$ as in Eq. (6.10). The leading contribution to the integral in Eq. (6.22) comes from the pole at $\omega = v_F k$. For small j , i.e. lattice sites close to the boundary, small k and small ω , $\tilde{\varphi}_k(j)/\tilde{\varphi}_{\tilde{\omega}}(j)$ depends only weakly on k and can thus be replaced by unity.

6.3.3 Spectral function

In the Appendix we partly solve the Lippmann-Schwinger equation for the off-shell K matrix Eq. (6.16) and present arguments which strongly suggest that the leading behavior of $g(\omega)$ and $h_1(\omega)$ for small $|\omega|$ is given by power-laws

$$g(\omega) = \left[\frac{U}{8\pi v_F} \right]^2 \left[\left| \frac{2\omega}{v_F k_F} \right|^{-\alpha_B^H} + \text{sign}(\omega) \right]^2, \quad (6.23)$$

and

$$h_1(\omega) = \left| \frac{2\omega}{v_F k_F} \right|^{-\alpha_B^H}. \quad (6.24)$$

The boundary exponent α_B^H is defined in Eq. (6.3). Using Eq. (6.19) for $|\omega| \ll v_F k_F$ the spectral function at the boundary site is thus given by

$$\rho_1^{\text{eff}}(\omega) \sim \frac{\left| \frac{2\omega}{v_F k_F} \right|^{-\alpha_B^H}}{1 + \left[\frac{U}{8v_F} \right]^2 \left[\left| \frac{2\omega}{v_F k_F} \right|^{-\alpha_B^H} + \text{sign}(\omega) \right]^2}. \quad (6.25)$$

The way the effective model was constructed this analytical result captures the leading small $|\omega|$ behavior of the local spectral function of the Hubbard model within the Hartree approximation. All the features found in our numerical calculations Sec. 6.2 and Ref. [29] are confirmed by Eq. (6.25). For $U > 0$ and $|\omega| \rightarrow 0$ we first find a power-law increase of the weight with exponent $-\alpha_B^H$ given by the numerator of Eq. (6.25). For even smaller $|\omega|$ the denominator becomes important and a power-law decrease with α_B^H sets in. From Eq. (6.25) the crossover scale Δ can be calculated analytically

$$\frac{\Delta}{v_F k_F} = \exp \left\{ -\frac{\pi v_F}{U} \ln \frac{1 + [U/(8v_F)]^2}{[U/(8v_F)]^2} \right\}. \quad (6.26)$$

Up to logarithmic corrections it is exponentially small in $-1/U$ as already expected from the numerical data. The $\text{sign}(\omega)$ function in the denominator of Eq. (6.25) is responsible for the asymmetry of the spectral weight around $\omega = 0$ discussed in Sec. 6.2.

The analytical result Eq. (6.25) makes clear that it was essential to determine the leading small $|\omega|$ behavior of the K matrix Eq. (6.16), respectively of $g(\omega)$ Eq. (6.21) and $h_j(\omega)$ Eq. (6.22), instead of the leading behavior of the T matrix: The latter one gives the final power-law decrease, but does not capture the power-law increase and the crossover.

For $U < 0$ only the numerator of Eq. (6.25) is relevant and leads to the symmetric power-law suppression of the weight close to μ with exponent $|U|/(2\pi v_F)$. This confirms the numerical results of Sec. 6.2.

We note in passing that by calculating the local spectral function of the 1D Hubbard model in the Hartree approximation, we have determined the local spectral function for the one-particle scattering problem of an electron in an external $\cos(2k_F x)/x$ potential. The Jost function and scattering matrix for this problem have recently been discussed in the literature[31].

7 Discussion and Summary

Our study of the one-particle properties of LL's with open boundaries covers different aspects of the low-energy physics of 1D electrons with repulsive interaction. We have carefully reinvestigated the bosonization approach to 1D models with OBC, especially focusing on the subtleties, which go beyond the ones known from bosonization of models with PBC. As no RG study exists which takes all the scattering processes into account we have restricted ourselves to interactions which are long range in real space and the low-energy subspace of the Fock space applying Tomonaga's original idea[2] to models with OBC. We were then able to confirm the result for the boundary exponent α_B which characterizes the suppression of spectral weight close to the boundary and the chemical potential[11]. $\alpha_B = (K_\rho^{-1} - 1)/z$ can indeed be expressed in terms of the bulk LL parameter K_ρ of the Tomonaga-Luttinger model. Led by this observation and analogy to PBC several authors have generalized the above results to all models of LL's[11, 12]. Using the numerically exact DMRG algorithm we investigated whether this is a legitimate generalization for two models with a short range interaction: The lattice model of spinless fermions with nearest neighbor interaction and the 1D Hubbard model[13, 14]. In both cases we were able to explicitly verify that the final suppression of the spectral weight at small energies is consistent with the prediction of bosonization, although for the Hubbard model only at energies surprisingly close to the chemical potential, respectively for very long chains.

Besides that our study has revealed two interesting new results. Firstly we found that many aspects of the influence a boundary has on the low-energy one-particle spectra can be understood within the Hartree-Fock approximation for the self-energy. Using numerical and analytical techniques we were able to explain how the non-trivial structure of the self-energy matrix leads to power-law behavior of the Hartree-Fock spectral function close to the boundary. For the two models with dominant forward scattering (TL model and lattice model of spinless fermions) quantitative agreement between the exact spectral function and the approximated one can be reached for small interactions. In both cases the exact boundary exponent α_B and α_B^{HF} agree up to leading order in the interaction and the energy range over which power-law behavior can be observed is large compared to the one observed in the Hubbard model.

The second surprising finding is the crossover behavior of the spectral function of the Hubbard model. In both the numerically exact DMRG calculation and the Hartree approximation the spectral weight for small and moderate U initially increases for energies approaching the chemical potential. Only below a crossover scale Δ the power-law suppression predicted by bosonization sets in. The DMRG data reveal that Δ strongly decreases with decreasing interaction U . Within the Hartree approximation we were able to show analytically that up to small corrections $\Delta = \Delta_0 \exp(-U_0/U)$, with $U_0 = \pi v_F$ and $\Delta_0 = v_F k_F$. Due to the scaling of coupling constants not captured in the Hartree approximation only qualitative agreement be-

tween the DMRG and Hartree spectral weight can be reached. The scaling is responsible for the fact that the Hartree boundary exponent α_B^H is twice as large as the leading behavior of the exact exponent. Furthermore the crossover scale is underestimated by the Hartree approximation (see Fig. 4 of Ref. [29]). Nonetheless we believe that the exact crossover scale shows an exponential $-1/U$ dependence, with a modified U_0 and Δ_0 . Within a perturbative RG calculation similar to “*g*-ology” we expect that irrelevant couplings scale to zero as $1/|\ln(\Lambda/\Lambda_0)|$ if $\Lambda \rightarrow 0$. Here Λ denotes the momentum scale up to which degrees of freedom have been integrated out and Λ_0 is the bare momentum cutoff (both measured relative to k_F). Thus irrelevant couplings scale down on exponentially (in $-1/U$) small scales. This implies that only Δ_0 and U_0 of the exponential dependence of Δ found in the Hartree approximation are modified. A similar result can be obtained if one starts at the LL fixed point and takes into account the anomalous dimension of the fermion field. Close to the LL fixed point the leading irrelevant couplings are expected to scale to zero as $(\Lambda/\Lambda_0)^{\gamma(U)}$, with $\gamma(U) \sim U$. This again leads to an exponential scale on which irrelevant couplings scale down. Our observation has dramatic implications for the energy range over which the prediction of bosonization is valid in the present context: It vanishes exponentially in $-1/U$.

The perturbative result Eq. (3.6) for the spectral weight indicates that the crossover behavior can be found in all models with dominant total backscattering $z\tilde{V}(2k_F) > \tilde{V}(0)$.

Over the past ten years several groups have attempted to find LL behavior in a variety of systems which behave as quasi one-dimensional conductors using angular integrated and angular resolved photoemission spectroscopy[19,20,21,22,23]. Here we do not want to give a complete account of all the experiments and the subtleties of their interpretation[19] and focus on one aspect, which we believe has to be reconsidered in the light of our results. The angular integrated spectra of all the possible candidates for LL behavior show a suppression of spectral weight close to the chemical potential[19]. If the data are interpreted in terms of the LL picture surprisingly large exponents α of the order of 1 are required. Within bulk LL theory this implies K_ρ 's smaller than the once for which umklapp scattering becomes relevant taking the filling factors of the experimental systems. This leads to a contradiction since the data do not show signs of a gap. Furthermore in a recent angular resolved measurement[20] the authors were unable to detect any dispersion of the peaks measured. Motivated by the theoretical expectation that a LL chain with impurities will, at low energies, behave as if it is cut into several disconnected pieces with open ends[9,10] both the missing dispersion and the large exponent have been interpreted in the light of this expectation. If the electrons come from localized regions of the chain, they do not display any dispersion. For electrons coming from positions close to an open boundary α_B would be the relevant exponent. As we have seen earlier $\alpha_B > \alpha$. This would resolve the apparent contradiction mentioned

above, since a α_B of the order of 1 can still lead to a K_ρ larger than the critical value at which umklapp scattering leads to a gapped system. Thus it has been speculated[12,14,19,20,23] that data have to be compared with calculations for LL's with open ends. As we have demonstrated above in these systems the energy range over which the LL exponent α_B can be observed might be very small and taking thermal and experimental broadening into account even masked by a pronounced peak at higher energies. At the lower end this energy range is furthermore cut off by non LL effects as e.g. interchain hopping[36]. For a variety of reasons our results can certainly not directly be applied to experimental spectra. One is that for the Hubbard model studied boundary exponents $\alpha_B \approx 1$ cannot be reached. What would thus be very desirable is a calculation of the boundary spectral weight in a microscopic lattice model with an interaction which is of longer range leading to boundary exponents of the order of one. We conclude that a convincing interpretation of the data in terms of boundary effects is still missing and requires further theoretical investigations.

We would like to thank A. Rosch and J. Voit for helpful discussions. This work has been supported by the SFB 341 of the Deutsche Forschungsgemeinschaft (V. M. and W. M.). Part of this work was performed while K.S. spent his sabbatical at the ICTP in Trieste. He would like to thank YU, Lu for the hospitality in his group. Part of the calculations were carried out on a T3E of the Forschungszentrum Jülich.

Appendix

In this appendix we will determine the leading small $|\omega|$ behavior of the functions $g(\omega)$ and $h_1(\omega)$ defined in Eqs. (6.21) and (6.22) from the solution of the Lippmann-Schwinger equation (6.16). For the dimensionless K matrix $\tilde{K}(\omega) = K(\omega)/v_F$ it reads

$$\left[\tilde{K}(\omega) \right]_{k,k'} = \tilde{\mathcal{V}}_{k,k'} + \rlap{-}\int_{-k_F}^{k_F} dp \frac{\tilde{\mathcal{V}}_{k,p} \left[\tilde{K}(\omega) \right]_{p,k'}}{\tilde{\omega} - p}, \quad (\text{A1})$$

with

$$\tilde{\mathcal{V}}_{k,k'} = \mathcal{V}_{k,k'}/v_F = -\tilde{U}\Theta(k+k'), \quad (\text{A2})$$

where $\tilde{U} = U/(4\pi v_F)$, and $\tilde{\omega} = \omega/v_F$. By differentiating Eq. (A1) with respect to k a system of coupled differential equations for

$$\mathcal{F}_1(k) \equiv \mathcal{F}_1(k; k', \omega) = \left[\tilde{K}(\omega) \right]_{k,k'} - \tilde{\mathcal{V}}_{k,k'} \quad (\text{A3})$$

and

$$\mathcal{F}_2(k) \equiv \mathcal{F}_2(k; k', \omega) = \mathcal{F}_1(-k; k', \omega) \quad (\text{A4})$$

can be derived

$$\mathcal{F}_1'(k) = \tilde{U}^2 \frac{\Theta(k' - k)}{\tilde{\omega} + k} - \tilde{U} \frac{\mathcal{F}_2(k)}{\tilde{\omega} + k}, \quad (\text{A5})$$

$$\mathcal{F}_2'(k) = -\tilde{U}^2 \frac{\Theta(k' + k)}{\tilde{\omega} - k} + \tilde{U} \frac{\mathcal{F}_1(k)}{\tilde{\omega} - k}. \quad (\text{A6})$$

The boundary conditions are $\mathcal{F}_1(-k_F) = \mathcal{F}_2(k_F) = 0$.

We did not succeed in analytically solving this system of differential equations for arbitrary k , k' , and small $|\omega|$. To determine the leading small $|\omega|$ behavior of $g(\omega)$ and $h_1(\omega)$ we fortunately only need $\mathcal{F}_1(k; k', \omega)$ for certain special combinations of the arguments. From Eqs. (A3) and (6.21) it follows that $g(\omega)$ is given by

$$g(\omega) = \left[\mathcal{F}_1(\tilde{\omega}; \tilde{\omega}, \omega) + \tilde{\mathcal{V}}_{\tilde{\omega}, \tilde{\omega}} \right]^2. \quad (\text{A7})$$

The differential equation (A6) can be used to express $h_1(\omega)$ Eq. (6.22) in terms of $\mathcal{F}_1(k_F; \tilde{\omega}, \omega)$ [35]

$$\begin{aligned} h_1(\omega) &= \left[1 + \mathcal{P} \int_{-k_F}^{k_F} dk \frac{\mathcal{F}_1(k; \tilde{\omega}, \omega) + \tilde{\mathcal{V}}_{k, \tilde{\omega}}}{\tilde{\omega} - k} \right]^2 \\ &= \left[1 + \frac{1}{\tilde{U}} \mathcal{P} \int_{-k_F}^{k_F} dk \mathcal{F}'_2(k) \right]^2 \\ &= \left[1 - \frac{1}{\tilde{U}} \mathcal{F}_1(k_F; \tilde{\omega}, \omega) \right]^2. \end{aligned} \quad (\text{A8})$$

We thus only have to evaluate $\mathcal{F}_1(k_F; \tilde{\omega}, \omega)$ and $\mathcal{F}_1(\tilde{\omega}; \tilde{\omega}, \omega)$ in the limit $|\omega| \ll v_F k_F$.

In a first step Eqs. (A5) and (A6) are solved for $\omega = 0$. In this case a new variable $t(k) = \ln |k|$ can be introduced and the equations can be decoupled by introducing $\mathcal{F}_\pm = \mathcal{F}_1 \pm \mathcal{F}_2$. The rest of the calculation is straightforward and leads for $|k| \geq |k'|$ to

$$\begin{aligned} \mathcal{F}_1(k; k', \omega = 0) &= \tilde{U} \Theta(k + k') \\ &- \frac{\tilde{U}}{2} \left[\left| \frac{k}{k_F} \right|^{-\tilde{U}} + \text{sign}(k) \left| \frac{k}{k_F} \right|^{\tilde{U}} \right] \left| \frac{k'}{k_F} \right|^{-\tilde{U}} \end{aligned} \quad (\text{A9})$$

For $|k'| > |k|$, k and k' have to be interchanged. If we set $k = k_F$, $k' = \tilde{\omega}$, and assume $|\omega| \ll v_F k_F$, Eq. (A9) simplifies to

$$\begin{aligned} \mathcal{F}_1(k_F; \tilde{\omega}, 0) &= \tilde{U} - \tilde{U} \left| \frac{\omega}{v_F k_F} \right|^{-\tilde{U}} \\ &= \tilde{U}^2 \ln \left| \frac{\omega}{v_F k_F} \right| - \frac{\tilde{U}^3}{2} \ln^2 \left| \frac{\omega}{v_F k_F} \right| + \dots \end{aligned} \quad (\text{A10})$$

The first few terms in the expansion in powers of \tilde{U} can easily be obtained by iterating the Lippmann-Schwinger equation (6.16) for the K matrix. Unfortunately the quantity presented in Eq. (A10) is not quite what is needed to calculate $h_1(\omega)$. An exact solution is difficult, but it is straightforward to calculate the first terms in the \tilde{U} expansion for $\left[\tilde{K}(\omega) \right]_{k_F, \tilde{\omega}}$. For $|\omega| \ll v_F k_F$ this yields

$$\mathcal{F}_1(k_F; \tilde{\omega}, \omega) = \tilde{U}^2 \ln \left| \frac{2\omega}{v_F k_F} \right| - \frac{\tilde{U}^3}{2} \ln^2 \left| \frac{2\omega}{v_F k_F} \right| + \dots$$

If we now assume that this expansion can be resummed as in Eq. (A10) we obtain

$$h_1(\omega) = \left| \frac{2\omega}{v_F k_F} \right|^{-2\tilde{U}}. \quad (\text{A11})$$

For $k = \tilde{\omega}$ and $k' = \tilde{\omega}$ Eq. (A9) gives

$$\begin{aligned} \mathcal{F}_1(\tilde{\omega}; \tilde{\omega}, 0) &= \tilde{U} \Theta(\omega) - \frac{\tilde{U}}{2} \left[\left| \frac{\omega}{v_F k_F} \right|^{-2\tilde{U}} + \text{sign}(\omega) \right] \\ &= \tilde{U}^2 \ln \left| \frac{\omega}{v_F k_F} \right| - \tilde{U}^3 \ln^2 \left| \frac{\omega}{v_F k_F} \right| + \dots \end{aligned} \quad (\text{A12})$$

Iteration of Eq. (6.16) for $\left[\tilde{K}(\omega) \right]_{\tilde{\omega}, \tilde{\omega}}$ leads to

$$\mathcal{F}_1(\tilde{\omega}; \tilde{\omega}, \omega) = \tilde{U}^2 \ln \left| \frac{2\omega}{v_F k_F} \right| - \tilde{U}^3 \ln^2 \left| \frac{2\omega}{v_F k_F} \right| + \dots$$

If we again assume that the logarithm can be summed to a power-law as in Eq. (A12) we obtain the result for $g(\omega)$ presented in Eq. (6.23).

References

1. For a review see: J. Voit, Rep. Prog. Phys. **58**, 977 (1995).
2. S. Tomonaga, Prog. Theor. Phys. **5**, 544 (1950).
3. J.M. Luttinger, J. Math. Phys. **4**, 1154 (1963).
4. D.C. Mattis, E.H. Lieb, J. Math. Phys. **6**, 304 (1965).
5. J. Sólyom, Adv. Phys. **28**, 201 (1979).
6. F.D.M. Haldane, J. Phys. C **14**, 2585 (1981).
7. H.J. Schulz, Phys. Rev. Lett. **64**, 2831 (1990).
8. S. Qin *et al.*, Phys. Rev. B **56**, 9766 (1997).
9. D.C. Mattis, J. Math. Phys. **15**, 609 (1974).
10. C.L. Kane, M.P.A. Fisher, Phys. Rev. Lett. **68**, 1220 (1992).
11. M. Fabrizio, A. Gogolin, Phys. Rev. B **51**, 17827 (1995).
12. S. Eggert, H. Johannesson, A. Mattsson, Phys. Rev. Lett. **76**, 1505 (1996).
13. Y. Wang, J. Voit, F.-C. Pu, Phys. Rev. B **54**, 8491 (1996).
14. J. Voit, Y. Wang, M. Grioni, preprint (1999).
15. G. Bedürftig *et al.*, Phys. Rev. B **58**, 10225 (1998).
16. Introductions to bosonization are given in K. Schönhammer, cond-mat/9710330 and J. von Delft, H. Schoeller, Ann. Phys. **7**, 225 (1998).
17. *Density-Matrix Renormalization*, ed. by I. Peschel *et al.* (Springer, Berlin, 1999) and references therein.
18. R. Preus *et al.*, Phys. Rev. Lett. **73**, 732 (1994).
19. For a recent review of the experimental situation see: M. Grioni, J. Voit, to be published in *Electron spectroscopies applied to low-dimensional materials*, ed. by H. Stanberg and H. Hughes (1999).
20. F. Zwick *et al.*, Phys. Rev. Lett. **79**, 3982 (1997).
21. J.D. Denlinger *et al.*, Phys. Rev. Lett. **82**, 2540 (1999).
22. J. Xue *et al.*, Phys. Rev. Lett. **83**, 1235 (1999).
23. P. Segovia *et al.*, Nature **402**, 504 (1999).
24. Here we only consider the case of an equal number of electrons with up and down spin.
25. T. Stauber, Diploma-thesis, Universität Göttingen, 1998.
26. As the Green's and spectral function are independent of the spin direction s we have suppressed the spin index.
27. Here we neglect all the problems which might occur due to local minima and maxima in $\xi(k)$ or bandedges.
28. K. Schönhammer, V. Meden, Phys. Rev. B **47**, 16205 (1993).

29. K. Schönhammer, V. Meden, W. Metzner, U. Schollwöck, O. Gunnarsson, cond-mat/9903121, to appear in Phys. Rev. B (February 2000).
30. For the Hubbard model the Fock term vanishes. Thus we write ρ^H instead of ρ^{HF} .
31. M. Klaus, J. Math. Phys. **32**, 163 (1991).
32. The leading behavior of K_ρ is given by $K_\rho = 1 - U/(2\pi v_F)$. Note the misprint in Eq. (8) of Ref. [7].
33. G. Schliecker *et al.*, J. Phys. Condens. Matter **7**, 7969 (1995).
34. J.R. Taylor, *Scattering Theory* (Wiley, New York, 1972).
35. Note that $\tilde{\varphi}_k(j)/\tilde{\varphi}_{\bar{\omega}}(j)$ in Eq. (6.22) has been replaced by 1.
36. P. Kopietz, V. Meden, K. Schönhammer, Phys. Rev. Lett. **74**, 2997 (1995); E. Arrigoni, Phys. Rev. Lett. **83**, 128 (1999).